Magnetic breakdown and quantum interference in the quasi-two-dimensional superconductor $\kappa-(BEDT-TTF)_2Cu(NCS)_2$ in high magnetic fields

1996 J. Phys.: Condens. Matter 8 5415

(http://iopscience.iop.org/0953-8984/8/29/016)

J. Phys.: Condens. Matter **8** (1996) 5415–5435. Printed in the UK

Magnetic breakdown and quantum interference in the quasi-two-dimensional superconductor κ-(BEDT-TTF)$_2$Cu(NCS)$_2$ in high magnetic fields

N Harrison†, J Caulfield‡, J Singleton‡, P H P Reinders†, F Herlach†, W Hayes‡, M Kurmoo§ and P Day§

† Laboratorium voor Vaste-Stoffysica en Magnetisme, Katholieke Universiteit Leuven, Celestijnenlaan 200D, B-3001 Heverlee, Belgium

‡ Physics Department, University of Oxford, Clarendon Laboratory, Parks Road, Oxford OX1 3PU, UK

§ The Royal Institution, 21 Albemarle Street, London W1X 4BS, UK

Received 19 March 1996

Abstract. Magnetic breakdown phenomena have been investigated in the longitudinal magnetoresistance of the quasi-two-dimensional (Q2D) superconductor κ-(BEDT-TTF)$_2$Cu(NCS)$_2$ in magnetic fields of up to 50 T, well above the characteristic breakdown field. The material is of great interest because its relatively simple Fermi surface, consisting of a closed Q2D pocket and an open Q1D band, is almost identical to the initial hypothetical breakdown network proposed by Pippard. Two frequencies are expected to dominate the magnetoresistance oscillations: the α frequency, corresponding to orbits around the closed pocket, and the β frequency, corresponding to the simplest classical breakdown orbit. However, a $\beta - \alpha$ frequency is in fact found to be the dominant high-frequency oscillation in the magnetoresistance. Numerical simulations, employing standard theories for calculating the density of states, indicate that a significant presence of the $\beta - \alpha$ frequency (forbidden in the standard theories) can result simply from the frequency-mixing effects associated with the pinning of the chemical potential in a quasi-two-dimensional system. While this effect is able to account for the previous experimental observation of $\beta - \alpha$ frequency oscillations of small amplitude in the magnetization, it cannot explain why such a frequency dominates the high-field magnetotransport spectrum. Instead we have extended the numerical simulations to include a quantum interference model adapted for longitudinal magnetoresistance in a quasi-two-dimensional conductor. The modified simulations are then able to account for most of the features of the experimental magnetoresistance data.

1. Introduction

Pulsed magnetic fields have proved to be a valuable experimental tool in the study of charge-transfer salts of the molecule bis(ethylenedithio)tetrathiafulvalene (abbreviated as BEDT-TTF or ET) [1–5]. On applying strong magnetic fields, the amplitudes of the quantum oscillatory phenomena such as the Shubnikov–de Haas (SdH) and de Haas–van Alphen (dHvA) effects are observed to grow rapidly, often showing departures from conventional Lifshitz–Kosevich (LK) behaviour as the quantum limit is approached [2, 3, 5, 6]. In this paper, magnetic fields of up to 50 T and temperatures between 350 mK and 4.2 K have been used to study the effects of magnetic breakdown (MB) and quantum interference (QI) in the charge-transfer salt κ-(BEDT-TTF)$_2$Cu(NCS)$_2$. The magnetic fields used comfortably exceed the characteristic MB field B_0, thus enabling the high-frequency quantum oscillatory features due to MB and related mechanisms to be resolved with great clarity.

0953-8984/96/295415+21$19.50

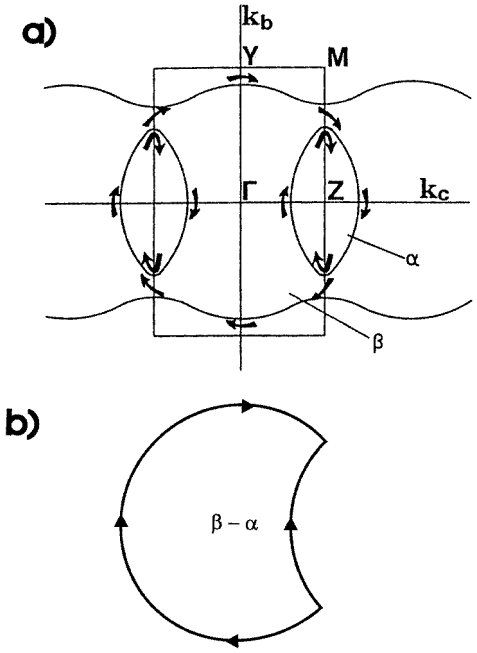

Figure 1. (a) The Fermi surface of κ-(BEDT-TTF)$_2$Cu(NCS)$_2$ in the b-plane comprising an open quasi-one-dimensional sheet and a closed pocket α (taken from [12]). The action of magnetic breakdown enables the 'free-electron-like' β orbit. (b) A schematic representation of the 'forbidden' $\beta - \alpha$ 'orbit.'

κ-(BEDT-TTF)$_2$Cu(NCS)$_2$ has attracted considerable interest over recent years, as it boasts one of the highest superconducting transition temperatures ($T_c = 10.4$ K) of any BEDT-TTF salt [7]. The salt has also been investigated using the dHvA effect in the vortex state [8] and SdH oscillations under hydrostatic pressure; the latter measurements enabled the first direct study of the relationship between the quasiparticle effective mass and T_c in any superconductor [9]. Band-structure calculations for this material predict a large quasi-two-dimensional (Q2D) Fermi surface pocket of holes [10]; following general usage we shall refer to quasiparticle orbits about this complete Fermi surface as the β orbit (see figure 1(a)). The dimerization of the BEDT-TTF molecules introduces an additional weak lattice potential in the reciprocal-lattice k_c-direction which has the effect of halving the Brillouin zone and splitting the Fermi surface into a Q2D lens pocket α and an open quasi-one-dimensional (Q1D) sheet (see figure 1(a)). Consequently, the α frequency dominates SdH and dHvA spectra at low magnetic fields; at higher fields, the β frequency plus a host of combination frequencies appear as a result of MB [11–13].

As will be seen in section 3 of this paper, in many respects the MB phenomena observed experimentally in κ-(BEDT-TTF)$_2$Cu(NCS)$_2$ agree with the standard network model [14–16]. Indeed, the geometry of the Fermi surface is almost exactly that of the hypothetical one-dimensional network model proposed by Pippard (see [14, 15]). However, significant differences from the standard network model are suggested by the experimental observation of the $\beta - \alpha$ frequency (see section 3 and [11, 12]), the existence of which requires a sudden reversal of the path of the quasiparticle along its semiclassical trajectory [16] (figure 1(b)). Given that this 'forbidden' frequency has been most commonly observed in

magnetotransport measurements [11, 12], its origin has been ascribed to the Stark quantum interference (QI) effect [17, 18]. It is well known [17, 18] that the Stark QI effect should not contribute to the free energy of the system and so the resultant frequencies should not be detected in the magnetization. However, the recent observation of weak oscillations with the $\beta-\alpha$ frequency in torque magnetometer measurements [13] has provoked further debate as to its origin [19].

The manifestation of a $\beta-\alpha$ frequency in the magnetization strongly suggests real oscillations of this frequency in other thermodynamic functions of state such as the free energy. In an attempt to explain the origin of the $\beta-\alpha$ frequency, Machida *et al* [19] recently performed numerical calculations in which they modelled the energy level structure of κ-(BEDT-TTF)$_2$Cu(NCS)$_2$ using an extension of the Hofstadter problem [20]. By including an additional weak lattice potential in the Hamiltonian they were able to introduce the effect of MB phenomena on the energy spectrum. A significant $\beta-\alpha$ frequency was found to be present in their simulations, and was therefore thought to be a consequence of the recursive band-structure picture [19].

Whilst the model proposed by Machida *et al* [19] may be a possible explanation for the $\beta-\alpha$ frequency, the possibility of more than one mechanism contributing to its existence cannot be ruled out. In contrast to the work of Machida *et al*, in section 4 of this paper we have calculated the magnetization and magnetoresistance numerically using the conventional schemes of Pippard (see [14, 15]) and Falicov and Stachowiak [16] for evaluating the density of states (DOS) in the presence of MB. Numerical calculations have the advantage that they enable effects such as the oscillatory chemical potential to be included; the oscillatory chemical potential has recently been shown to give rise to deformation of the waveform [6] and to frequency-mixing effects in BEDT-TTF charge-transfer salts at high magnetic fields [5]. The results of the calculations in section 4 indicate that the pinning of the chemical potential to sharply defined Landau levels is responsible for the observation of the $\beta-\alpha$ frequency in magnetization measurements.

Magnetotransport data differ significantly from magnetization data in that the $\beta-\alpha$ frequency is much stronger and the relative spectral weights of all frequencies are different. In section 5 of this paper we have adapted the original theories of Stark QI [17, 18] for the purpose of modelling the longitudinal magnetoresistance of κ-(BEDT-TTF)$_2$Cu(NCS)$_2$. By making a number of assumptions and approximations, the effects of QI can be included within the calculations of the longitudinal magnetoresistance, to give a satisfying qualitative explanation of the experimental results in section 3.

2. Experimental details

The single crystal of κ-(BEDT-TTF)$_2$Cu(NCS)$_2$ used in this experiment was a hexagonal platelet of approximate dimensions $0.3 \times 0.4 \times 0.2$ mm^3 (the shortest dimension is perpendicular to the conducting Q2D planes), synthesized using standard electrochemical procedures [7, 10]. In some experiments, the sample was oriented with the magnetic field perpendicular to the conducting (Q2D) *bc*-planes; however, the majority of experiments were performed with the magnetic field rotated by an angle of 13° from the axis normal to the conducting planes. This orientation was chosen because the SdH oscillations exhibit a spin maximum (i.e. the cosine damping term in the LK formula due to spin splitting of the Landau levels is 1) close to this angle, thereby rendering them most clearly observable [13]. The effects of MB are not sensitive to small angular displacements. The magnetoresistance was measured in the longitudinal configuration by applying the current perpendicular to the conducting planes. Four 20 μm gold wires were attached to the sample using platinum

paint, giving typical two contact resistances of ∼10 Ω. Experiments were performed using an alternating current of 25 μA at 250 kHz; trial measurements with higher currents demonstrated that this value caused negligible heating of the sample. The signal detection system, pulsed field magnet and ^{3}He cryostat have been described in detail elsewhere [5]; in the context of this paper we merely note that the field pulse is asymmetric, possessing lower values of $\mathrm{d}B/\mathrm{d}t$ on the falling side than on the rising side. The signal-to-noise ratio is therefore generally higher on the falling side of the magnetic field pulse and so in the following sections we shall only show data obtained under these conditions.

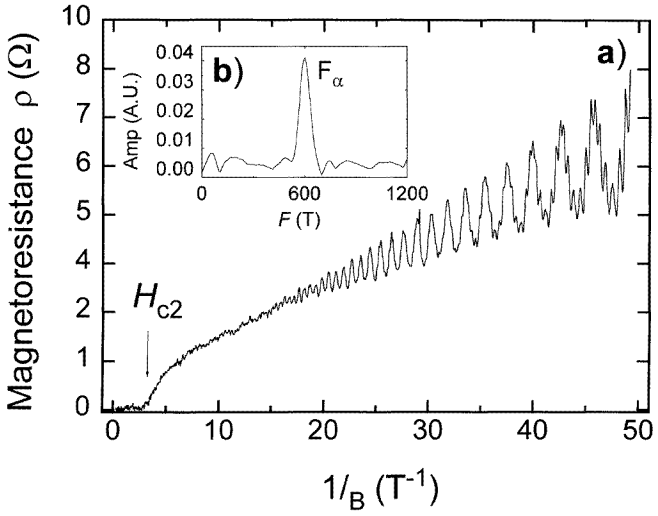

Figure 2. (a) An example of a longitudinal magnetoresistance trace at 350 mK, with the magnetic field at an angle of 13° with respect to the reciprocal-lattice vector $\boldsymbol{a}^*$. (b) A Fourier transform of a data trace recorded at the 0° orientation at 1 K. This yields the fundamental frequency of the α orbit.

3. Results

3.1. General features

Figure 2(a) shows the magnetoresistance of the κ-(BEDT-TTF)$_2$Cu(NCS)$_2$ crystal at 350 mK; the sample surface normal is tilted by 13° with respect to the magnetic field. Apart from the superconducting–normal-state transition, which occurs between 3 and 6 T (such a broadened transition appears to be an intrinsic feature of the material; see [8] and references therein), the approximately temperature-independent background magnetoresistance increases linearly with no apparent saturation, reaching ∼6 Ω at 50 T. The principal SdH oscillations corresponding to the α orbit emerge above the background noise at ∼15 T, growing steadily in amplitude with increasing magnetic field. At higher magnetic fields, the previously observed higher frequencies associated with the $\beta-\alpha$, β, $\beta+\alpha$ and $\beta+2\alpha$ orbits due to MB and/or QI effects [9, 10] grow in amplitude, becoming comparable in size to the slower oscillations at 50 T. A Fourier transform of the quantum oscillations in the magnetoresistance (with the field tilted by 13° with respect to the sample surface normal) is shown in figure 3 and the frequencies are tabulated in table 1. As expected for

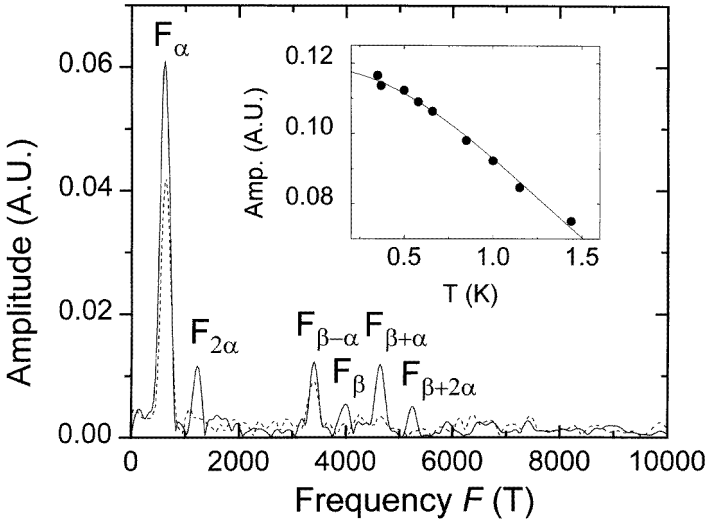

Figure 3. The solid line shows a Fourier transform of the raw data in figure 2(a) for the region of $1/B$ between 0.02 and 0.03 T^{-1}, after dividing by the background magnetoresistance. The dashed line shows the equivalent Fourier transform for data recorded at 1.44 K. Of the frequencies originating from magnetic breakdown, the $\alpha - \beta$ and $\alpha + \beta$ clearly dominate. The inset shows the temperature dependence of the α frequency amplitude. A fit has been made to the Lifshitz–Kosevich amplitude reduction factor R_T; the corresponding parameters are given in table 1.

a Q2D system [21], the frequencies shown in table 1 are shifted up by a factor $1/\cos(13^\circ)$ with respect to those of previous measurements [8–13] carried out with the magnetic field perpendicular to the sample Q2D planes. The measurements performed at 0° (figure 2(b)) yielded frequencies in close agreement with the previous measurements and are also listed in table 1.

Table 1. A list of the observed Shubnikov–de Haas and quantum interference frequencies with their associated effective masses. The effective masses shown are for the tilt angle of 13°.

Orbit	F (T) at 13°	F (T) at 0°	m^* (m_e)
α	626 ± 1	603 ± 5	3.5 ± 0.1
2α	1246 ± 4	—	6.4 ± 0.6
$\beta - \alpha$	3399 ± 3	3310 ± 8	3.6 ± 0.3
β	4026 ± 9	—	7.1 ± 0.5
$\beta + \alpha$	4652 ± 3	—	8.2 ± 0.4
$\beta + 2\alpha$	5279 ± 8	—	8 ± 3
2β	8131 ± 10	—	—

3.2. Effective-mass estimates

Effective masses were determined by fitting to the temperature reduction factor $R_T = X/\sinh[X]$ ($X \sim 14.69 m^* T/B$) from the conventional LK expression [15, 22]; an example of such a fit is shown in the inset to figure 3. The effective masses derived in this way

are shown in table 1; these are also shifted up by the small factor $1/\cos(13^\circ)$ from the values derived for the field perpendicular to the Q2D planes [21]. Although the data used in deriving the masses include the oscillations up to the highest magnetic fields, the mass value for the α orbit is in close agreement with previous estimates. This agreement, together with the apparent good fit to the function R_T, suggests that the departures from LK behaviour due to the quasi-two-dimensionality of the Fermi surface (i.e. due to the chemical potential becoming pinned to very sharp Landau levels [6]) are not as significant in κ-(BEDT-TTF)$_2$Cu(NCS)$_2$ as they are, for example, in α-phase BEDT-TTF salts such as α-(BEDT-TTF)$_2$MHg(NCS)$_4$ (M = NH_4, K) [2, 3, 6]. The most likely explanation for this observation is that the Landau levels are broadened substantially, not only by the finite quasiparticle lifetime, but also by the effects of magnetic breakdown; we shall return to this point in the discussion in the following sections. However, the effective mass derived for the second harmonic of the α orbit oscillations ($6.4m_e$, where m_e is the free-electron mass) is slightly lower than twice the effective mass of the fundamental frequency ($3.5m_e$); in the LK formalism, the second-harmonic mass is exactly twice that of the fundamental. The unexpectedly low mass for the second harmonic has also been noted in other works involving high magnetic fields, for instance [11–13]. Moreover, the principal α frequency oscillations are distinctly peaked in appearance (see figure 4(a); the maxima are narrower than the minima, so the oscillations do not appear sinusoidal). Both of these observations suggest that a small departure from LK behaviour is occurring at high magnetic fields [6]. Nevertheless, we stress that such effects are much more extreme in α-(BEDT-TTF)$_2$$NH_4$Hg(NCS)$_4$, where very strongly peaked SdH oscillations are observed in the magnetoresistance due to near-insulating behaviour when the chemical potential is at energies between very sharply defined Landau levels [3, 6].

3.3. Phase analysis and interference effects

According to the theory of Falicov and Stachowiak [16], MB introduces an additional damping factor $R_{B,j} = p^{n1_j} q^{n2_j} \exp[\mathrm{i}\, n1_j\phi_p + \mathrm{i}\, n2_j\phi_q]$ for each of the frequencies j involved, where $P = p^2 = \exp[-B_0/B]$ is the characteristic breakthrough probability and $q^2 = 1 - p^2$. The integers $n1$ and $n2$ denote the number of points of magnetic breakthrough and Bragg reflection encountered along the semiclassical trajectory of the quasiparticle orbit respectively. Since the phases of the 'free electron' and Bragg reflected waves are in quadrature following a breakdown junction [14–16], we therefore have $\phi_p + \phi_q = \pm\pi/2$. In contrast to the case for three-dimensional metals such as Hg in which additional arbitrary contributions are added to the Onsager phase due to the curvature of the Fermi surface [15, 16], in a Q2D system the situation is much simpler, providing an opportunity for the phase of the oscillations to be determined with more certainty.

In a two-dimensional metal with MB, the oscillatory contribution of each orbit to the DOS is given, according to Falicov and Stachowiak [16], by

$$\tilde{g}_j = 2\frac{N}{\varepsilon_F} C \frac{m^*}{m^*_\beta} p^{n1} q^{n2} (-1)^{l'_j} \cos\left[l_j\phi_j[\varepsilon] + n1\phi_p + n2\phi_q\right] \mathrm{e}^{-\pi l_j/\omega_j\tau}. \qquad (1)$$

Here, N is the total carrier density, ω_j is the characteristic cyclotron frequency and τ^{-1} is the quasiparticle scattering rate. ϕ_j is the Onsager phase, which for a parabolic band depends linearly on ε. For the main β orbit, we have assumed that the energy ε is zero at the bottom of the band. At the Fermi energy ε_F, the phase of this orbit is $\phi_j = 2\pi F_j/B$, where F_j is the characteristic dHvA frequency. The weight factor C_j accounts for the number of times that each orbit occurs in the Brillouin zone. In this model l_j is the harmonic index whilst

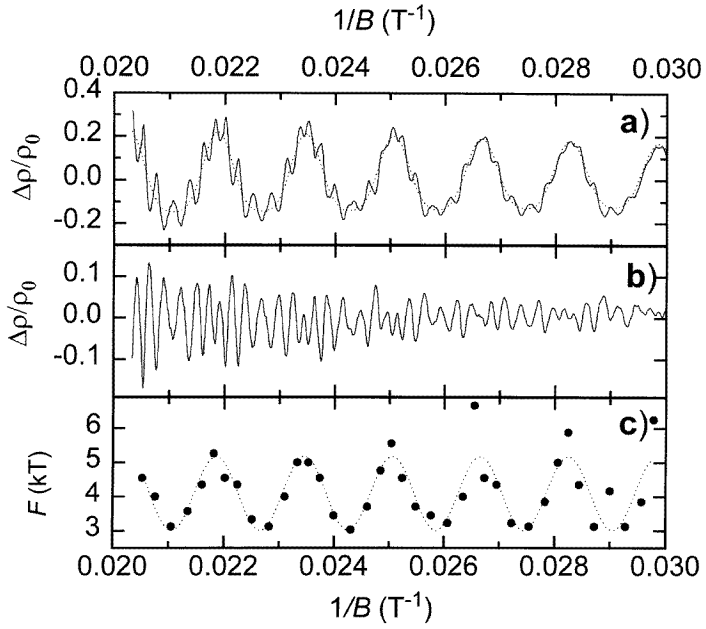

Figure 4. (a) A plot of the quantum oscillations versus $1/B$ (solid line), after dividing by the background magnetoresistance, together with a fit made to the fundamental and second harmonic of the α frequency (dotted line). (b) The higher-frequency components of the oscillations after the fit made in figure 4(a) has been subtracted. (c) A plot of the interval of $1/B$ between oscillation maxima versus $1/B$. A sinusoidal fit through the points strongly suggests a correlation of this 'frequency modulation' effect with the waveform of the α orbit oscillations in figure 4(a).

l'_j is the number of times that a wavepacket passes the same point on the Fermi surface throughout its semiclassical trajectory. This distinction may appear trivial but is in fact important; e.g. in the case of the $\alpha + \beta$ orbit, $l_j = 1$ whereas $l'_j = 2$.

In the absence of MB (i.e. where q tends to zero), equation (1) leads to minima in the DOS at integer values of $\varepsilon/\hbar\omega_c$ or F/B; in standard magnetotransport theory [23, 24] these DOS minima result in maxima in the longitudinal magnetoresistance. This is indeed observed in the case of α-phase BEDT-TTF salts [6], where the magnetoresistance maxima appear to correspond to the chemical potential being located in or close to the gap between two adjacent Landau levels. In contrast, for the α orbit in κ-(BEDT-TTF)$_2$Cu(NCS)$_2$ (figure 4(a)) peaks in the magnetoresistance occur at values $\varepsilon/\hbar\omega_c = r - (0.287 \pm 0.001)$, where r is an integer. The origin of this additional phase shift is unclear, but the fact that a phase shift of this kind is not seen in the α-phase BEDT-TTF salts suggests that it may be a product of the MB effect [25].

Figure 4(b) shows the high-frequency component of the SdH oscillations for the field interval between 30 and 50 T; the fundamental and second harmonic of the α orbit SdH oscillations have been subtracted using the fit shown in figure 4(a) (this fit was made using parameters derived from the Dingle analysis in the following section). The remaining fast oscillations comprise a complicated beat of the $\beta - \alpha, \beta, \beta + \alpha$ and $\beta + 2\alpha$ frequencies. A close inspection of the fast oscillations reveals that higher-frequency oscillations appear to coincide with the peaks in the magnetoresistance (i.e. peaks in the α orbit oscillations), whilst lower-frequency oscillations coincide with the magnetoresistance minima. Figure 4(c)

shows the reciprocal of the interval of $1/B$ between the neighbouring maxima in figure 4(b) plotted as a frequency $F = (1/B_{\max 2} - 1/B_{\max 1})^{-1}$ versus $1/B$. A sinusoidal fit through these points (figure 4(c)) suggests that the frequency modulation of the high-frequency oscillations is closely correlated with the waveform of the low-frequency SdH oscillations due to the α orbit (figure 4(a)). The mean oscillation frequency is that of the β orbit to within experimental errors, whilst the difference between the minimum and the maximum frequencies is approximately $3.5\,F_\alpha$. We shall return to a discussion of this feature of the magnetoresistance in section 5, which covers the theoretical modelling of QI effects.

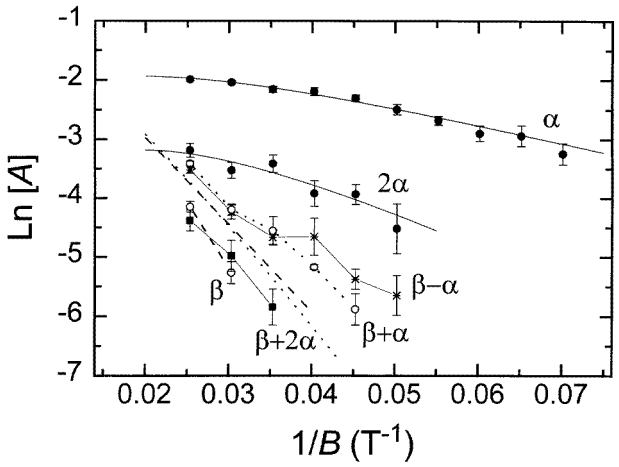

Figure 5. Dingle plots of the observed frequencies. Where necessary, the points have been connected by straight lines in order to show which points belong to the same orbit. The smooth solid lines represent a fit to the first and second harmonics of the α orbit amplitude. The smooth dashed and dotted lines correspond to the expected amplitudes of the β and $\beta + \alpha$ frequencies respectively, according to the Falicov and Stachowiak model for magnetic breakdown [16].

3.4. Amplitude analysis

By convention, the field dependence of the amplitude of SdH oscillations is analysed by plotting the function

$$\ln[A] = \ln\left[\left(\frac{\Delta\rho}{\rho_0}\right)\frac{\sinh X}{X}\right] \tag{2}$$

versus $1/B$, where $\Delta\rho$ and ρ_0 are the oscillatory and background components of the magnetoresistance respectively. This usually results in a linear graph (a so-called Dingle plot) from which the Dingle temperature T_D can be determined [15, 26]. Owing to the combined effects of MB and the slight departures from LK behaviour due to the quasi-two-dimensionality of the Fermi surface, the corresponding Dingle plots for κ-(BEDT-TTF)$_2$Cu(NCS)$_2$ in figure 5 show some degree of deviation from a straight line. Of these two effects, MB is the most prominent [6], leading to a downward adjustment of the Dingle plot by an amount $\Delta\ln[A] = \ln\left[p^{n1_j}q^{n2_j}\right]$, where both p and q are dependent on the magnetic field. A fit of the equation $\ln[A] = \ln[A_{0,j}] - \gamma_j/B - \ln\left[p^{n1_j}q^{n2_j}\right]$ to the Dingle plot requires the adjustment of three parameters: $\gamma = 2\pi^2 l k_B T_{D,j} m_j^*/\hbar e$, B_0 and the infinite-field intercept $\ln[A_0]$. Owing to close functional correlations between

the latter two terms, a fit to the first harmonic alone cannot produce a satisfactory fit. However, a simultaneous fit to both the first and second harmonics yields the parameters $T_{D,\alpha} = 0.64 \pm 0.04$ K, $B_0 = 41 \pm 7$ T and $\ln[A_{0,\alpha}] = -0.7 \pm 0.1$. The integrity of the fit depends on the extent to which the LK formalism is able to approximate the behaviour of the low-frequency oscillations in this material. The small deviation of the effective mass $m^*_{2\alpha} = 6.4m_e$ from the expected value of $7m_e$ in this case suggests that the assumption of the validity of the LK theory will only result in a small error. Nevertheless, the characteristic breakdown field determined here is somewhat higher than those determined from the 'low'-field SdH measurements of Caulfield *et al* [9] and the dHvA measurements of Meyer *et al* [13]. The difference between these results and that in the present work is most likely an indication of the difficulties in obtaining a reliable value of the breakdown field using only low-field data; the fits in figure 5 show that in order to gain a reasonable estimate one needs to observe MB at magnetic fields exceeding the breakdown field.

Using the parameters derived above for the quasiparticle scattering rate and characteristic breakdown field, in figure 5 we have calculated the expected Dingle plots for the β and $\beta+\alpha$ frequencies according to the standard MB theory of Falicov and Stachowiak [16]. Clearly, the amplitude of the β orbit is somewhat smaller than that expected from the theory, while that of the $\beta + \alpha$ frequency is somewhat enhanced. The overall slopes of the Dingle plots, however, appear to be roughly consistent with the MB theory. The change of the relative amplitudes of the standard breakdown frequencies is therefore likely to be associated with the same effects (whether frequency mixing or QI) which are responsible for the generation of the $\beta - \alpha$ frequency; we shall return to this point in section 5 of this paper.

4. Numerical simulations of magnetic breakdown excluding quantum interference

4.1. The model

In this section of the paper, we consider the influence of the quasi-two-dimensionality of the Fermi surface on the frequency content of the oscillations. In high magnetic fields, the Landau levels of Q2D metals become well separated in energy, leading to an oscillatory chemical potential which can give rise to frequency-mixing effects [5, 6]. This problem is not easily tractable by analytical means; the oscillatory chemical potential, Landau level broadening and finite temperature plus the effects of MB must be included in calculations of the thermodynamic function of state. A complete summation over all energy states is required which is most conveniently evaluated using numerical calculations [6]. Since the Fermi surface of κ-(BEDT-TTF)$_2$Cu(NCS)$_2$, depicted in figure 1(a), corresponds very closely to the one-dimensional network model proposed by Pippard (see [14, 15]), the latter's result forms a convenient point of departure; i.e.

$$\cos[\omega] = \frac{\cos\left[\frac{1}{2}\phi_\beta\right] + q^2\cos\left[\frac{1}{2}\phi_\beta - \phi_\alpha\right]}{\left|2q\cos\left[\frac{1}{2}\phi_\alpha\right]\right|}. \tag{3}$$

Here, ω is the characteristic phase change of a quasiparticle on passing from a given point on the Fermi surface to the equivalent point in the next Brillouin zone [14, 15], and ϕ_α and ϕ_β are the Onsager phases of the α and β orbits respectively. Equation (3) is obtained by accounting for all of the phases and amplitudes of the quasiparticles crossing the Brillouin zone boundary (where the two β orbits of neighbouring zones intersect); see figure 7.4 of [14], which results in a set of simultaneous (or coupled) equations. For simplicity we have assumed the phase shift associated with magnetic breakthrough to be 90° (as did Pippard) [14, 15]. Since $\cos[\omega]$ lies only between -1 and $+1$ for real ω, equation (3) can be used

to generate the spectrum of permitted states, either in energy space or magnetic field space. In order to account for the zero-point energy (which was ignored in Pippard's original calculations; see [14, 15]) and to make equation (3) compatible with LK theory [15, 22], π has been added to the Onsager phases in equation (3). This results in the substitution of the function 'cos' for the function 'sin' which was in Pippard's original equation; see [14, 15]. Consequently, in the limit where q tends to zero, equation (3) reproduces the spectrum corresponding to the free-electron case with only the β orbit present. In the opposite limit as q tends to 1, a virtually continuous distribution of states is obtained, corresponding to the Q1D open Fermi surface on top of which the α orbit Landau level states are superimposed.

It is convenient to approximate the main Fermi surface element (β orbit) in figure 1(a) by a parabolic band; hence the Onsager phase

$$\phi_\beta = \frac{2\pi m^*_\beta \varepsilon}{e\bar{h}B} \tag{4}$$

is linear with energy. In figure 1(a), the extremal area of this band intersects the zone boundary at a distance $K_C/2$ from the centre of the zone, where K_C is the reciprocal-lattice constant in this direction. If we assume this band to have a circular geometry (i.e. have the same radii in the k_b and k_c lattice directions), we can calculate the area and hence the phase of the resultant α pocket to be

$$\phi_\alpha = \mathrm{Re}\left[\frac{2\pi m^*_\beta \varepsilon}{e\bar{h}B}\left(\cos^{-1}[z] - z\sqrt{1-z^2}\right)\right] \tag{5}$$

where $z = \sqrt{\bar{h}^2 K_C^2/8\varepsilon m^*_\beta}$. The effective mass of each orbit is given by $m^*_j = \partial A_j/\partial\varepsilon$, where the area $A_j = eB\phi_j/\bar{h}$ [14, 15]; for the α orbit this can be obtained by differentiation of equation (5) to yield $m^*_\alpha = (2m^*_\beta/\pi)\cos^{-1}[z]$. At $\varepsilon = \varepsilon_F$ this has the value $0.5\,m^*_\beta$; note that the experimental masses (table 1) obey this relationship to within ~10%, illustrating the close correspondence between the Fermi surface of κ-(BEDT-TTF)$_2$Cu(NCS)$_2$ and Pippard's model. A further useful proportionality is that the effective mass of an orbit is proportional to its perimeter. Under the constraint that the extremal area of the β orbit is equal to the total area of the Brillouin zone, we can define the Fermi energy as $\varepsilon_F = \bar{h}^2 K_B K_C/2\pi m^*_\beta$. By inserting the known crystallographic parameters $K_C \approx 4.9 \times 10^9$ m^{-1} and $K_B \approx 7.5 \times 10^9$ m^{-1} [7, 10], we obtain $F_\beta \sim 3850$ T and $F_\alpha \sim 660$ T; these frequency values are close to the experimentally determined frequencies [11–13].

Since the spectrum of allowed energy states can be calculated at equally spaced intervals of ω (as was done by Pippard) [14, 15], we can use equation (3) to obtain the DOS in the limit where $\tau^{-1} = 0$. Consequently, each increment of ω by π corresponds to exactly one Landau level; hence it can be shown that $g[\varepsilon, B] = \mathrm{Re}|(\mathrm{d}\omega/\mathrm{d}\varepsilon)NB/\pi F_\beta|$. By inserting the Onsager phases given by equations (4) and (5), the DOS can be calculated. In figure 6 we show an example of the DOS as a function of magnetic field for the case where the chemical potential is constant (i.e. equal to the Fermi energy ε_F). The distribution of the states can be seen to be broadened, even without a finite quasiparticle scattering time. For the case of a finite scattering rate, the DOS can be calculated using the result of Falicov and Stachowiak [16] (i.e. equation (1)).

With the DOS having been obtained, the chemical potential μ can be obtained in the normal manner by inverting the integral

$$N = \int_\varepsilon g[\varepsilon, B] f[\varepsilon - \mu]\,\mathrm{d}\varepsilon \tag{6}$$

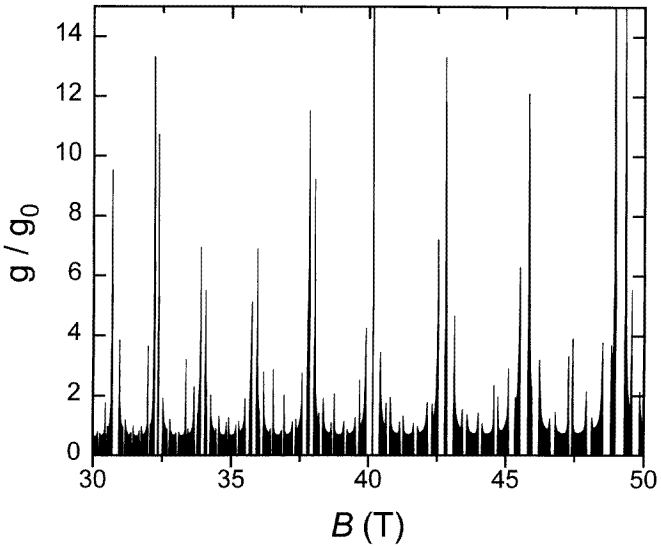

Figure 6. A plot of the density of states at the Fermi energy (which is constant) as a function of the magnetic field, calculated using equation (3). The points where the states are clustered together more intensively (i.e. of greater degeneracy) correspond to the Landau levels of the α orbit. The Landau levels corresponding to all of the magnetic breakdown frequencies are contained within the general distribution of states.

numerically, where $f[\mu - \varepsilon]$ is the Fermi–Dirac distribution function. The free energy is given by

$$H_F = \mu N - kT \int_{\varepsilon} g[\varepsilon, B] \ln\left[1 + \mathrm{e}^{(\mu-\varepsilon)/kT}\right] \mathrm{d}\varepsilon. \tag{7}$$

4.2. Calculations of the magnetization

Figure 7(a) shows the computed free energy at temperatures of 0.4 and 1.4 K for the field range between 30 and 50 T, using the DOS obtained from equations (3)–(7) (i.e. zero scattering rate). At the lowest temperatures, the higher frequencies of the MB are superimposed on the principal α frequency oscillations; closer inspection reveals that they are cusp-shaped. Figure 7(b) shows the corresponding magnetization calculated via the relation $M = -\partial H_F/\partial B$. In many respects, the calculated magnetization waveform is comparable to that experimentally observed by Meyer *et al* [13], in that the higher-frequency oscillations have a larger amplitude on the rising slope of the magnetization than on the falling slope. Fourier analysis of the calculated magnetization, shown in figure 7(c) [27], reveals the presence of a significant $\beta - \alpha$ frequency and even a further weak feature at $\beta - 2\alpha$. Since the conventional MB theory described above does not allow such frequencies, the $\beta - \alpha$ and $\beta - 2\alpha$ frequencies must therefore be solely a result of the effect of the oscillations of the chemical potential on the thermodynamic functions. For comparison, figure 7(d) shows the Fourier transform of the equivalent magnetization calculated using the same numerical procedure but with the chemical potential held constant (i.e. analogous to the standard LK approach). This latter result is in full agreement with the conventional spectrum predicted by the network model; note that the $\beta - \alpha$ and $\beta - 2\alpha$ frequencies

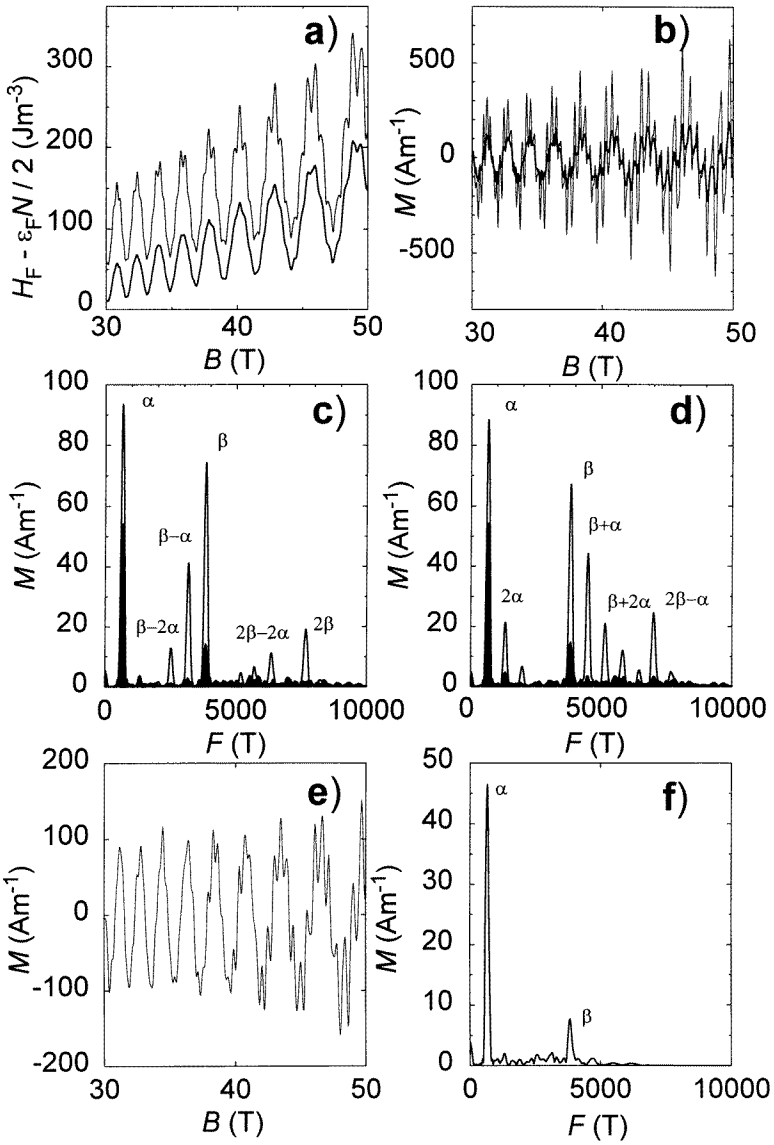

Figure 7. (a) The computed free energy H_F for the temperatures 0.4 K (thin line) and 1.4 K (thick line). (b) The corresponding magnetization obtained by differentiating figure 7(a). (c) The Fourier transform of the oscillations in figure 7(b) at 0.4 K (unshaded) and 1.4 K (shaded), revealing a significant presence of the $\beta - \alpha$ and $\beta - 2\alpha$ frequencies. (d) The equivalent Fourier transform of the magnetization calculated in the same manner but with the chemical potential held constant. (e) The magnetization calculated at 0.4 K for the scattering rate appropriate for the measurements of this work. (f) The corresponding Fourier transform.

are absent.

It is now possible to see how the $\beta - \alpha$ and $\beta - 2\alpha$ frequencies come to be present in the magnetization when μ is allowed to oscillate [13]. As stated above, the higher-frequency MB oscillations occur predominantly on the rising slope of the magnetization

(see figure 7(b) and figure 2(a) of [13]) due to the fact that the phases of the β and $\beta+\alpha$ orbits interfere constructively at this point on the waveform. Furthermore, it is on the rising slope of the magnetization where the chemical potential is 'pinned' to the Landau levels associated with the α orbit. The pinning of the chemical potential has the effect of causing the energy levels of the β and $\beta+\alpha$ orbits to pass through the chemical potential more slowly; i.e. as the chemical potential moves up with the α orbit Landau levels, features due to the β and $\beta+\alpha$ orbits are shifted to lower frequencies by an amount close to the α orbit frequency.

In many respects, the Fourier transform of figure 7(c) is very similar indeed to that obtained by Machida *et al* [19], even insofar that the $\beta+\alpha$ frequency is vanishingly small in both cases. Since the chemical potential was allowed to oscillate in the model in [19], it seems likely that the $\beta-\alpha$ and $\beta-2\alpha$ frequencies in the results of those calculations are an artefact of the oscillatory chemical potential rather than a general property of the Hamiltonian.

By comparison of figure 7(c) with 7(d), it can be seen that the effects of the oscillatory chemical potential become less important at higher temperatures; i.e. the shaded Fourier transforms corresponding to 1.4 K are essentially the same. For this reason, the amplitude of the $\beta-\alpha$ frequency drops off strongly with increasing temperature; exactly the same is true when a finite quasiparticle scattering is introduced. In figure 7(e) we show the calculated magnetization using the quasiparticle scattering rate obtained in section 3 (i.e. $\tau^{-1}=0.53\pm0.03\times10^{12}$ s^{-1}), and in figure 7(f) we show the corresponding Fourier transform. It is clear from figure 7(f) that the $\beta-\alpha$ frequency has become vanishingly small, and this probably explains why the $\beta-\alpha$ frequency was only weakly present in the measurements of Meyer *et al* on κ-(BEDT-TTF)$_2$Cu(NCS)$_2$ [13]. Owing to its strong temperature dependence, the $\beta-\alpha$ frequency in the magnetization should have an apparent very heavy 'effective mass'. However, in section 5 it will become apparent that the temperature dependence of the amplitude of magnetoresistance oscillations of this frequency will be rather different.

4.3. Calculations of the magnetoresistance

In section 4.2, it was demonstrated that allowing the chemical potential to vary with field results in the presence of the $\beta-\alpha$ frequency in the oscillations of thermodynamic quantities such as the magnetization. However, none of the above calculations are able to give a $\beta-\alpha$ frequency which is the dominant high-frequency oscillation. Whilst the calculations are similar to experimental *magnetization* data, this feature is in marked contrast to the experimental *magnetoresistance* data, in which oscillations of the $\beta-\alpha$ frequency are often the most intense after those of the α orbit (see figure 3 of this work and also data shown by Caulfield *et al* [11]). In an attempt to understand this contrast between magnetization and magnetoresistance experiments, we shall in the remainder of this section calculate the magnetoresistance using the results of equations (3)–(7). It will be seen that this simple theory is unable to reproduce the predominance of the $\beta-\alpha$ frequency. Instead, the effects of quantum interference must be introduced, and this will be carried out in section 5.

In contrast to calculations of the magnetization, which is a thermodynamic function of state and therefore a direct consequence of the electronic density of states, the evaluation of the magnetoresistance depends on many assumptions about complex transport scattering processes and the exact geometry of the Fermi surface. For instance, the structure of the magnetoresistance quantum oscillations will depend strongly on the direction of the current with respect to the magnetic field. Usually in Q2D organic conductors the longitudinal

magnetoresistance is measured, therefore requiring theories which deal specifically with the longitudinal SdH effect. Most theories which treat this geometry deal with three-dimensional systems [23]. The reason for this is simple; by definition, there is no longitudinal conductivity in strictly 2D systems. The Q2D organic conductors represent a class of materials of intermediate dimensionality, having some properties in common with semiconductor superlattices [24]. Laikhtman and Menashe [24] have recently calculated the oscillatory longitudinal magnetoresistance for semiconductor superlattices in the low-magnetic-field limit. The fact that the oscillatory magnetoresistance is smaller than the background magnetoresistance in figure 2 implies that the low-magnetic-field limit is appropriate for our measurements. For this case, we can calculate the magnetoresistance using the approximate formula [6, 23, 24]

$$\sigma_z = -\sigma_{z,0} \int_\varepsilon \left(1 + \lambda \frac{\Delta g}{\bar{g}}\right) f'[\varepsilon] \, \mathrm{d}\varepsilon. \tag{8}$$

Here, $f'[\varepsilon]$ is the derivative with respect to energy of the Fermi–Dirac distribution and Δg and $\bar{g}$ are the oscillatory and background components of the DOS respectively. λ is a dimensionless constant of order unity which will be model dependent. In the case of a constant chemical potential, the integration over energy in equation (8) simply results in the familiar R_T reduction factor in the LK formalism [15, 22]. In the present case, however, the effects of the oscillatory chemical potential at high magnetic fields must be included; the integration must be performed numerically, taking into account the dependence of $f'[\varepsilon]$ on μ [28].

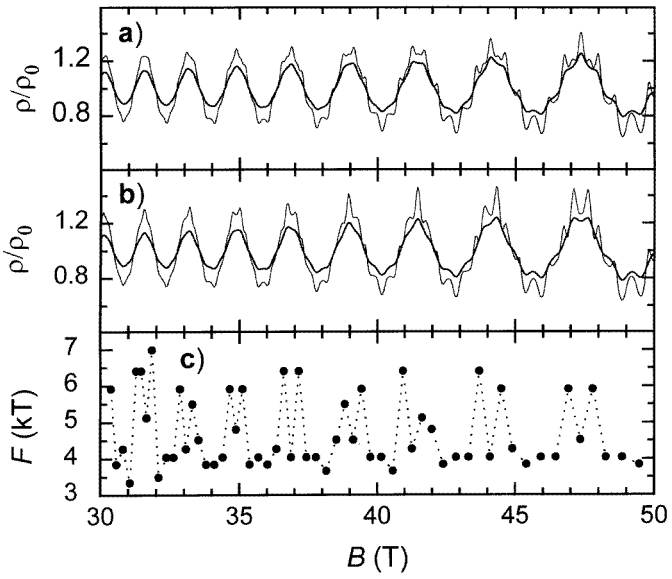

Figure 8. (a) The longitudinal magnetoresistance calculated using the simple model defined by equation (8). (b) The magnetoresistance calculated including the effects of quantum interference using equation (16). (c) A plot of the interval in $1/B$ between the calculated resistance maxima in figure 8(c). The correlation with the phase of the α oscillations in figure 8(c) is similar to that observed experimentally.

Figure 8(a) shows the magnetoresistance for κ-(BEDT-TTF)$_2$Cu(NCS)$_2$ calculated assuming the relation $\rho_z = 1/\sigma_z$ and using equation (1) for the DOS. A quasiparticle

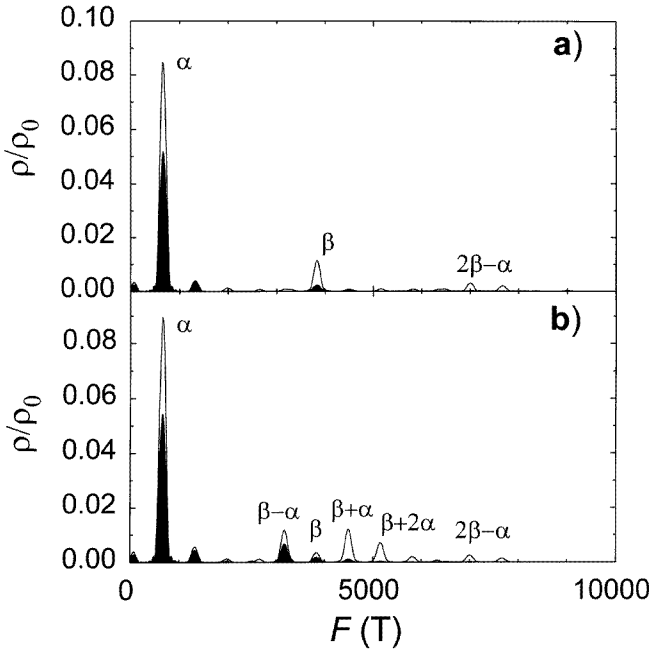

Figure 9. (a) A Fourier transform of the longitudinal magnetoresistance calculated in figure 8(a) assuming the simple model without the effects of quantum interference. A striking feature of this result is the dominance of the β frequency over its nearest neighbours, which contradicts experimental observations. (b) The corresponding Fourier transform of the calculated longitudinal magnetoresistance in figure 8(b) with the inclusion of quantum interference effects in accordance with the approximate model summarized by equation (16). The strong presence of the $\beta-\alpha$ and $\beta+\alpha$ frequencies is strikingly similar to that experimentally observed in figure 3.

scattering rate ($\tau^{-1} = (0.53 \pm 0.03) \times 10^{12}$ s^{-1}) and temperatures appropriate for the measurements in this work have been used, and for simplicity λ has been assumed to be 1. While the relative magnitude of the high-frequency oscillations is comparable to those observed experimentally in figure 4(a), the frequency modulation effects do not appear to be present in the calculations. Fourier transformation of the magnetoresistance, shown in figure 9(a), reveals that the β frequency dominates the high-frequency spectrum, and that the amplitudes of the $\beta-\alpha$, $\beta+\alpha$ and $\beta+2\alpha$ frequencies are vanishingly small. Clearly, the results of this calculation contrast greatly with the experimental results shown in figure 3. Nevertheless, the Fourier transform in figure 9(a) is comparable to that calculated for the magnetization in figure 7(f), in which quasiparticle scattering has been included; within the LK formalism, we should expect the magnetoresistance and magnetization spectra to be comparable.

5. Quantum interference effects

In the final part of section 4 it was shown that the standard longitudinal magnetoresistance models fail to produce a significant $\beta-\alpha$ frequency, let alone one which dominates the high-frequency spectrum. This implies that a more thorough calculation of the magnetoresistance requires the summation over all possible quasiparticle paths. With the inclusion of MB into

the problem, the number of possible paths becomes infinitely greater. The possibility of a quasiparticle having two or more possible paths between two points in real space leads to the occurrence of Stark QI.

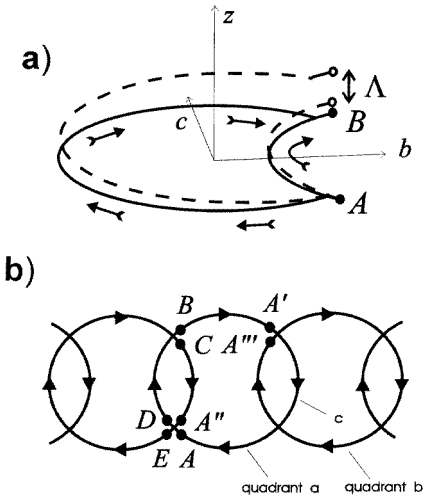

Figure 10. (a) The solid line illustrates the semiclassical motion of a quasiparticle along two of the possible paths between A and B, which leads to the $\beta - \alpha$ interference frequency. Owing to the quasi-two-dimensionality of the Fermi surface, there is often a longitudinal component of the velocity, leading to the trajectories shown by dashed lines. The difference in lengths of the paths leads to a relative displacement Λ in real space between the interfering quasiparticles. (b) A schematic diagram of the possible starting positions A and recombination points B, C, D and E which lead to the quantum interference effects.

In this section we begin our treatment of the Stark QI effect by considering the approach of Morrison and Stark [18]. The full calculation of the magnetoconductivity involves solving the linearized Boltzmann equation

$$\boldsymbol{\sigma} = e^2 \int \frac{\mathrm{d}^3 k}{4\pi^3} (-f') \boldsymbol{v}_k \boldsymbol{\Lambda}_k \tag{9}$$

where the quantity $\boldsymbol{\Lambda}_k$ is the k-averaged mean free displacement obtained by summing over all possible paths through the network

$$\boldsymbol{\Lambda}_k = \int_{-\infty}^{t_0} \boldsymbol{v}_k \mathrm{e}^{(t-t_0)/\tau_t} \, \mathrm{d}t. \tag{10}$$

The integration for each $\boldsymbol{k}$-vector is made over the evolutionary time t as the quasiparticle moves throughout the coupled network. For the purpose of calculating the transverse component of the conductivity, as was considered by Morrison and Stark (with the current orthogonal to the applied magnetic field), the transverse mean free displacement of a quasiparticle can be related to its k-space equivalent path $\boldsymbol{K}_k$, by the identity

$$\boldsymbol{\Lambda}_{k\perp} = \frac{\overline{h}}{eB} \hat{\boldsymbol{B}} \times \boldsymbol{K}_k. \tag{11}$$

While this is true for the transverse component of the magnetoresistance, the longitudinal component of the mean free displacement is different for the two branches of the interference orbit (see figure 10(a)). In a three-dimensional system, this will prevent QI from occurring

in the longitudinal direction. However, owing to the small component of the group velocity in the longitudinal direction in Q2D systems such as κ-(BEDT-TTF)$_2$Cu(NCS)$_2$, the path travelled (for example between points A and B in figure 10(b)) in that direction will be shorter than the longitudinal de Broglie wavelength [29]. This enables QI effects to be observed in the longitudinal magnetoresistance of κ-(BEDT-TTF)$_2$Cu(NCS)$_2$.

Table 2. The principal 'unique' orbits resulting from the effect of quantum interference. $|G'|$ and $|G''|$ have been written out in full, so as to indicate the paths taken. C_j takes into account the number of possible occurrences of the equivalent orbit within the Brillouin zone, divided by the four possible starting positions (A, A′, A″ and A‴); the actual route and the order in which the junctions of magnetic breakthrough or Bragg reflection are encountered may be different. The quantity $\bar{\lambda}_j$ in this table is the approximate relative average component of the path length travelled in the longitudinal direction; it has been renormalized to the distance covered on one revolution of the β orbit. Possibilities where the two branches of the quasiparticle orbit travel together along the same piece of Fermi surface or pass simultaneously through the same junction (in the same direction) do not count, since these possibilities are already comprised within other orbits.

Route	$\|G'\|$	$\|G''\|$	Orbit	C_j	m'_j	m^*_j	$\bar{\lambda}_j$ (relative)
A to B	pp	qp^2q	$\beta-\alpha$	2	m_β	$m_\beta-m_\alpha$	0.5
A to B	pp	qpq^2pq	β	4	$m_\beta+m_\alpha$	m_β	0.75
A to B	pp	qpq^4pq	$\beta+\alpha$	6	$m_\beta+2m_\alpha$	$m_\beta+m_\alpha$	1
A to B	pp	qpq^6pq	$\beta+2\alpha$	8	$m_\beta+3m_\alpha$	$m_\beta+2m_\alpha$	1.25
A to B	pq^2p	qp^2q	$\beta-2\alpha$	2	$m_\beta+m_\alpha$	$m_\beta-2m_\alpha$	0.75
A to B	pq^2p	qpq^2pq	$\beta-\alpha$	4	$m_\beta+2m_\alpha$	$m_\beta-m_\alpha$	1
...	...	...	...	...	...	...	...
A to D	pq	p^3q	β	1	m_β	m_β	0.5
A to D	pq	pq^2p^2q	$\beta+\alpha$	2	$m_\beta+m_\alpha$	$m_\beta+m_\alpha$	0.75
A to D	pq	pq^4p^2q	$\beta+2\alpha$	3	$m_\beta+2m_\alpha$	$m_\beta+2m_\alpha$	1
...	...	...	...	...	...	...	...
A to E	q	$-pqp$	α	1/2	m_α	m_α	0.25
A to E	q	$-pq^3p$	2α	1/2	$2m_\alpha$	$2m_\alpha$	0.5
...	...	...	...	...	...	...	...
A″ to C	q	$-p^3qp^3$	$2\beta-\alpha$	1/2	$2m_\beta$–m_α	$2m_\beta$–m_α	0.75
...	...	...	...	...	...	...	...

For the purpose of our calculations, it is necessary to resolve the longitudinal component of the mean free displacement into two components; hence

$$\Lambda_{k_z} = \bar{\Lambda}_{k_z} + \tilde{\Lambda}_{k_z}. \tag{12}$$

Since the action of MB does not affect the longitudinal motion of the quasiparticle, the average mean free displacement will always be given by the classical approximation: $\bar{\Lambda}_{k_z} = v_{k_z}\tau_{t,z}$ (in general, the longitudinal component of the velocity v_{k_z} depends on k_z). The oscillatory component $\tilde{\Lambda}_{k_z}$ includes only the interference terms. A full calculation of the magnetoresistance in any direction poses an intractable problem, even for the most elementary Fermi surface. However, we can approximately take into account the effects of QI using the following method; apart from those which are scattered with relatively short path lengths, all quasiparticles on the quadrant a of the Fermi surface (in figure 10(b)) inevitably pass the point A. From there on the wave splits, to be recombined later at the points B, C, D and E. By considering all possible trajectories between A and the recombination points, we can identify the principal paths which will lead to 'interference orbits' (see table 2 for a list). Each pair of interfering paths contributes a characteristic

Fourier component to $\tilde{\Lambda}_{k_z}$. For each branch of the interference orbit, we can define the wave amplitude propagator

$$G = p^{n1} q^{n2} \mathrm{e}^{\mathrm{i}\phi - t/2\tau} \tag{13}$$

where ϕ is the evolutionary phase of the quasiparticle (see [14] and [15]). The total probability amplitude upon reaching the point B on the Fermi surface will therefore be given by $P = |G' + G''|^2$, where G' and G'' are the wave amplitudes corresponding to the short and long paths respectively. Having reached B (for example), the exact point at which the quasiparticle is scattered is not important. In reality, the wave may continue to subdivide as it continues its motion through further magnetic breakthrough nodes. By this time, however, the wave will be considerably attenuated, so as a first approximation we can ignore these second-order QI effects.

The non-oscillatory component $\bar{P}$ contributes only to $\bar{\Lambda}_{k_z}$, which in our model is independent of the magnetic field. A small amount of algebra leads to the following expression for the oscillatory contribution to the probability amplitude:

$$\tilde{P}_j = 2 p^{n1_j} q^{n2_j} \cos[\phi_j] \mathrm{e}^{-\pi/\omega_j' \tau}. \tag{14}$$

Here, $n1$ and $n2$ denote the total number of points of magnetic breakthrough and Bragg reflection for both paths, while ϕ_j is the relative phase difference between the orbits, which appears as a virtual 'Onsager phase'. The effect of quasiparticle scattering leads to dephasing of the interference, so by analogy with the LK formalism the effective cyclotron mass $m_j' = eB/\omega_j'$ is proportional to the total perimeter of the interference orbit in k-space.

To calculate the total oscillatory contribution to the mean free displacement, we need to consider not only the recombination points B, C, D and E in figure 10(b), but also the other possible starting points A′, A″ and A‴. Of these A″ is symmetrically equivalent to A, and A′ and A‴ are mutually equivalent. Finally,

$$\tilde{\Lambda}_{k_z} \approx \sum_j C_j \bar{\lambda}_j \tilde{P}_j \tag{15}$$

where C_j is a weight which takes into account the number of occurrences of equivalent 'orbits' within the Brillouin zone, divided by the number of starting points. We can approximate $\bar{\lambda}_j \sim v_z/2\omega_j$ as the average of the lengths of the two interfering paths in the longitudinal direction. In reality, there will be some minor modification of equation (15) owing to the fact that a small percentage of the quasiparticles originating from quadrant a will be scattered before reaching point A in figure 10(b). This will lead to a small amplitude reduction factor. Intuitively, one might expect this effect to be compensated by a small number of non-scattered, non-interfering quasiparticles arriving from the quadrants b and c.

Even with this rather approximate treatment of the quantum interference effects in κ-(BEDT-TTF)$_2$Cu(NCS)$_2$, a full calculation of the magnetoconductivity using equation (9) represents a formidable problem. However, since the ratio $\tilde{\Lambda}_{k_z}/\bar{\Lambda}_{k_z}$ is independent of k_z within the model, the effects of QI can be included approximately as a correction factor $K_{QI} = (1 + \tilde{\Lambda}_{k_z}/\bar{\Lambda}_{k_z})$. Thus equation (8) can be rewritten as

$$\sigma_z = -\sigma_{z,0} \int_\varepsilon K_{QI} \left(1 + \lambda \frac{\Delta g}{\bar{g}}\right) f'[\varepsilon] \, \mathrm{d}\varepsilon. \tag{16}$$

The integration over ε implies that each interference frequency will have an associated thermal damping factor. The corresponding effective mass m_j^* which enters into the thermal damping factor is proportional to the difference in length between the two interfering paths in k-space, and is therefore different from the effective mass which enters into

the quasiparticle scattering term. In [18], the two interfering paths in metallic Mg have virtually equal lengths, leading to an effective mass of zero. For the $\beta - \alpha$ frequency in κ-(BEDT-TTF)$_2$Cu(NCS), the path lengths are not equal and the corresponding effective mass is $m^*_{\beta-\alpha} = m^*_\beta - m^*_\alpha \sim 3.6m_e$; this result agrees reasonably well with the experimental results.

In figure 8(b) we have calculated the magnetoresistance by means of equation (16), including all of the frequencies and parameters listed in table 2. The corresponding Fourier transform in figure 9(b) now shows many similarities with the experimental Fourier transform of figure 3. As observed experimentally, at higher temperatures the $\beta - \alpha$ frequency dominates the MB spectrum owing to its lower effective mass. At lower temperatures, the $\beta + \alpha$ interference frequency becomes increasingly dominant, perhaps explaining why the amplitude of the $\beta + \alpha$ frequency in figure 5 was larger than expected. Owing to the fact that the β SdH frequency and the β QI frequency are in anti-phase, the overall amplitude of this frequency is reduced, accounting for the suppression of the β frequency in the experimental results. Whilst the SdH frequency contains an additional phase factor of π due to the zero-point energy, such a phase factor is not expected to occur in QI effects [18].

In section 3 of this paper, it was noted that the higher-frequency oscillations (see figures 4(b) and 4(c)) exhibit a frequency modulation effect. The pattern of this interference effect is characteristic of the relative phase and amplitude relationships between the various interfering frequencies. In figure 8(b), the same procedure has been applied to the calculated trace, i.e. the reciprocal of the interval of $1/B$ between adjacent peaks has been plotted against $1/B$. Whilst it is evident from figure 8(c) that there exists some degree of correlation of the frequency F with the waveform in figure 8(b), the functional form is not as smooth as the experimental result in figure 4(c).

SdH oscillations with the $\beta - 2\alpha$ frequency were not directly observed in the current experiment, but have been observed experimentally by Kartsovnik *et al* [30]. For large oscillatory amplitudes (i.e. high-quality samples with low scattering), the product $K_{QI}(1 + \lambda\tilde{g}/\bar{g})$ in equation (16) can also lead to further frequencies such as $\beta - 2\alpha$ due to frequency-mixing effects. According to the values listed in table 1, the effective mass of this orbit should be $m^*_{\beta-2\alpha} = 0.1 \pm 0.5m_e$ (i.e. approximately zero).

6. Summary

We have investigated the effects of MB and QI at high magnetic fields in the charge-transfer salt κ-(BEDT-TTF)$_2$Cu(NCS)$_2$. By performing experiments above the characteristic breakdown field, the structure of quantum oscillations becomes clearly resolved, enabling comparisons with theoretical models. One of the major objectives has been to find the real origin of the $\beta - \alpha$ frequency, which is normally forbidden by standard theories for MB. Numerical calculations have shown that the oscillations of the chemical potential at high magnetic fields can explain the presence of a significant $\beta - \alpha$ frequency in the magnetization spectrum. However, this effect alone is not sufficient to explain the presence of a $\beta - \alpha$ frequency in the longitudinal magnetoresistance which dominates higher-frequency spectral content. Rather, the oscillations of the chemical potential lead to a suppression of all other frequencies in the magnetoresistance spectrum in favour of the β frequency.

The presence of a strong $\beta - \alpha$ frequency in the longitudinal magnetotransport spectrum can therefore only be explained by the Stark QI effect. Since the established theories deal only with QI in the transverse magnetoresistance, some adaptation of the theory is required in order to calculate its effect on the longitudinal magnetoresistance. The slow

longitudinal component of the quasiparticle velocity in the longitudinal direction enables the phase coherence in this direction between the departing wave amplitudes to be maintained. Calculations of the magnetoresistance including the effects of QI can thus be performed, and can successfully reproduce many aspects of the experimental data—in particular, the relative amplitudes of the various interference frequencies.

Acknowledgments

NH is a postdoctoral fellow of the Onderzoeksraad, KU Leuven. This work has received financial support from the EPSRC and the Royal Society (UK), and the Belgian NFWO.

References

[1] Singleton J, Pratt F L, Doporto J M, Caulfield J M, Hill S O, Janssen T J B M, Deckers I, Pitsi G, Herlach F, Hayes W, Perenboom J A A J, Kurmoo M and Day P 1993 *Physica* B **184** 470
[2] Harrison N, House A, Deckers I, Caulfield J, Singleton J, Herlach F, Hayes W, Kurmoo M and Day P 1995 *Phys. Rev.* B **52** 5584
[3] Sandhu P S, Athas G J, Brooks J S, Haanappel E G, Goette J D, Rickel D W, Tokumoto M, Kinoshita N, Kinoshita T and Tanaka Y 1996 unpublished
[4] Osada T, Yagi R, Kawasumi A, Kagoshima S, Miura N, Oshima M and Saito G 1990 *Phys. Rev.* B **41** 5428
[5] House A, Harrison N, Blundell S J, Deckers I, Singleton J, Herlach F, Hayes W, Perenboom J A A J, Kurmoo M and Day P 1996 *Phys. Rev.* B **53** 9127
[6] Harrison N, Bogaerts R, Reinders P H P, Singleton J, Blundell S J and Herlach F 1996 to be published
[7] Urayama H, Yamochi H, Saito G, Nozawa K, Sugano T, Kinoshita M, Sato S, Oshima K, Kawamoto A and Tanaka J 1988 *Chem. Lett.* (No 1) 55
[8] van der Wel P J, Caulfield J, Corcoran R, Day P, Hayden S M, Hayes W, Kurmoo M, Meeson P, Singleton J and Springford M 1994 *Physica* C **235** 2453
van der Wel P J, Caulfield J, Hayden S M, Singleton J, Springford M, Meeson P, Hayes W, Kurmoo M and Day P 1995 *Synth. Met.* **70** 831
[9] Caulfield J, Lubczynski W, Lee W, Singleton J, Pratt F L, Hayes W, Kurmoo M and Day P 1995 *Synth. Met.* **70** 815
Caulfield J, Lubczynski W, Pratt F L, Singleton J, Dyk K O, Hayes W, Kurmoo M and Day P 1994 *J. Phys.: Condens. Matter* **6** 2911
[10] Oshima K, Mori T, Inokuchi H, Urayama H, Yamochi H and Saito G 1988 *Phys. Rev.* B **38** 938
[11] Caulfield J, Singleton J, Pratt F L, Doporto M, Lubczynski W, Hayes W, Kurmoo M, Day P, Hendriks P T J and Perenboom J A A J 1993 *Synth. Met.* **61** 63
[12] Sasaki T, Sato H and Toyota N 1990 *Solid State Commun.* **76** 507; 1991 *Physica* C **185–189** 2687
[13] Meyer F A, Steep E, Biberacher W, Christ P, Lerf A, Jansen A G M, Joss W, Wyder P and Andres K 1995 *Europhys. Lett.* **32** 681
[14] Pippard A B 1962 *Proc. R. Soc.* A **270** 1; 1965 *Proc. R. Soc.* A **287** 165
[15] See also:
Shoenberg D 1984 *Magnetic Oscillations in Metals* (Cambridge: Cambridge University Press)
[16] Falicov L M and Stachowiak H 1966 *Phys. Rev.* **147** 505
[17] Stark R W and Reifenberger R 1977 *J. Low Temp. Phys.* **26** 763
[18] Morrison D and Stark R W 1981 *J. Low Temp. Phys.* **45** 531
[19] Machida K, Kishigi K and Hori Y 1995 *Phys. Rev.* B **51** 8946
[20] Hofstadter D R 1976 *Phys. Rev.* B **14** 2239
Hasegawa Y, Lederer P, Rice T M and Wiegmann P B 1989 *Phys. Rev. Lett.* **63** 907
[21] Doporto M, Pratt F L, Singleton J, Kurmoo M and Hayes W 1992 *Phys. Rev. Lett.* **69** 991
[22] Lifshitz I M and Kosevich A M 1956 *Zh. Eksp. Teor. Fiz.* **29** 730
[23] Argyres P N 1958 *J. Phys. Chem. Solids* **4** 19
Kubo R, Miyake S J and Hashitsume N 1965 The quantum theory of galvanomagnetic effect at extremely strong magnetic fields *Solid State Physics* vol 17, ed F Seitz and D Turnbull (New York: Academic) p 269
[24] Laikhtman B and Menashe D 1995 *Phys. Rev.* B **52** 8974
[25] One intriguing possibility is that it can be attributed to the phase shift ϕ_q which accompanies Bragg reflection. By convention, this has been chosen to be 0° in the standard theories [14–16], whilst the phase change

upon magnetic breakdown is 90°. If we identify the experimental phase shift with the quantity $n2\phi_q$ in equation (1), then since $n2 = 2$ for the α orbit, we infer that the phase change of a wavepacket upon Bragg reflection is $\phi_q \approx 50°$. However, such an effect is without precedent; for example the most prominent SdH oscillations in the α-phase (BEDT-TTF) salts involve four Bragg reflections and yet no comparable phase shifts are seen. Therefore MB appears to be the most likely cause of this effect in the current work (Dr Anton Polisskii, private communication).

[26] Dingle R B 1952 *Proc. R. Soc.* A **211** 500

[27] The 'apparent' noise in the Fourier transforms of figure 7 originates from errors in the calculation of the free energy. This is due mainly to the limited resolution in energy space to which the DOS was calculated.

[28] In recent calculations of the longitudinal magnetoresistance in α-phase BEDT-TTF salts [6] the formula $\sigma_z = \sigma_{z,0}\int(1+\Delta g/\bar{g})^2 f'\,\mathrm{d}\varepsilon$ was derived for SdH oscillations in high magnetic fields in the case where the oscillatory magnetoresistance was comparable in size to or bigger than the classical background magnetoresistance. The derivation of the formula involved assumptions which are valid specifically for the Q2D closed section of the Fermi surface of the α-phase BEDT-TTF salts [6]; the effects of MB were not included. The use of equation (8), which is generally valid under the conditions stated, therefore seems more appropriate.

[29] In [6], the maximum possible longitudinal component of the velocity (in the middle of the longitudinal band) was determined to be ∼300 m s^{-1}. For one revolution of the β orbit (for example) this corresponds to a longitudinal displacement of ∼1 nm at 40 T. In comparison, the de Broglie wavelength will always be longer than the longitudinal lattice parameter ∼1.6 nm.

[30] Kartsovnik M V *et al* 1995 *Int. Symp. on Crystalline Organic Metals, Superconductors and Ferromagnets (ISCOM)*